2.4 Comparison with analytical, numerical and laboratory results

A number of numerical experiments were performed to validate our method. The first experiment was to compare this solution with the exact nonlinear theory solution of Synolakis (1986, 1987a).

The topography used in the numerical computations and in Synolakis (1987) consist of a constant depth area and a plane sloping beach of angle β as shown in Figure 2.1. The initial conditions for the computations were solitary wave surface profiles of height H propagating in the positive x-direction and centered at $x = X_1$,

$$\eta(x,0) = \frac{H}{d}\operatorname{sech}^2\sqrt{\frac{3H}{4d}}(x - X_1) \tag{2.20}$$

and the initial wave particle velocities are defined by

$$u(x,0) = \eta(x,0)\sqrt{\frac{g}{d}}\ . \tag{2.21}$$

Equation (2.21) is the linear approximation of the depth-averaged particle velocities of the wave. To check the effect in the computation using this approximation, the solution with (2.21) was compared with a solution with an initial wave profile (2.20) with zero velocity. The latter initial condition produced two waves of the same shape and half of the initial amplitude propagating in opposite directions. Interestingly, we found no difference in the re-

sults between these two initial conditions, so we did not use a higher order approximation of $u(x, 0)$.

The center of the initial solitary wave profile was located at a distance L from the toe of the beach, where L is a measure of the half width of a solitary wave and

$$L = \sqrt{\frac{4d}{3H}}\,\mathrm{arccosh}\left(\sqrt{\frac{1}{0.05}}\right), \tag{2.22}$$

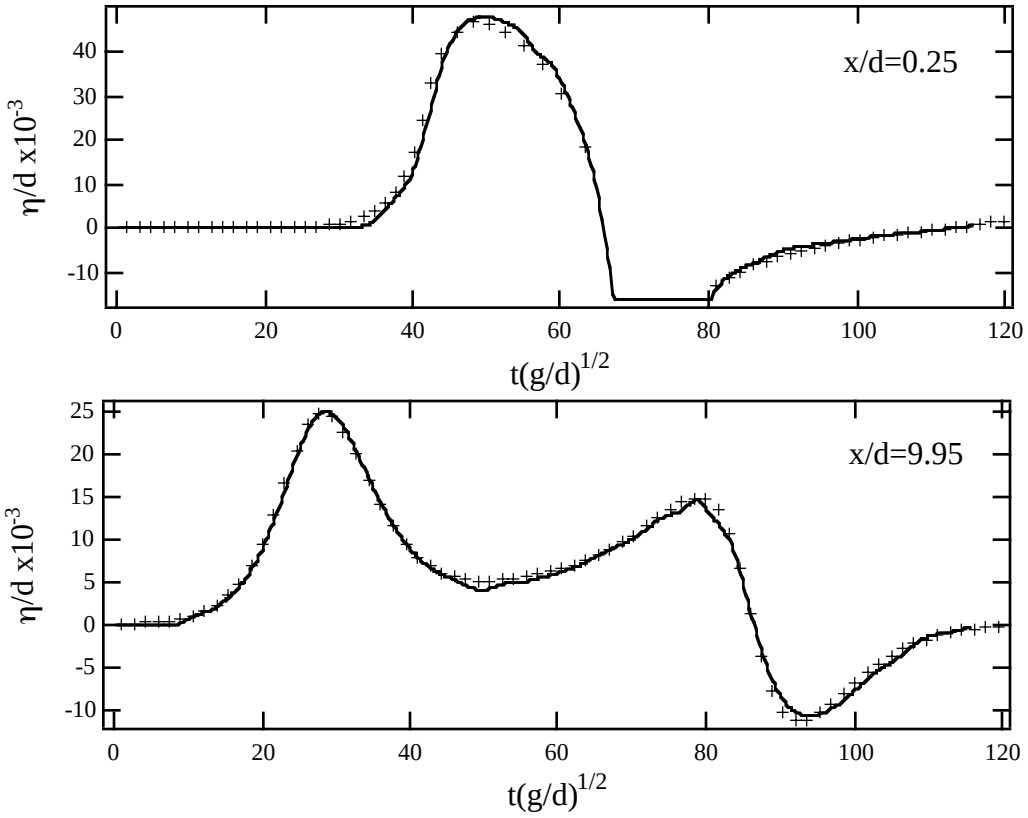

Figure 2.6 The evolution of a nonbreaking solitary wave with *H/d = 0.019* on a 1:19.85 beach. The normalized surface elevations are shown as a functions of the normalized time at two different locations; the solid line is the numerical solution, the crosses are the analytical results.

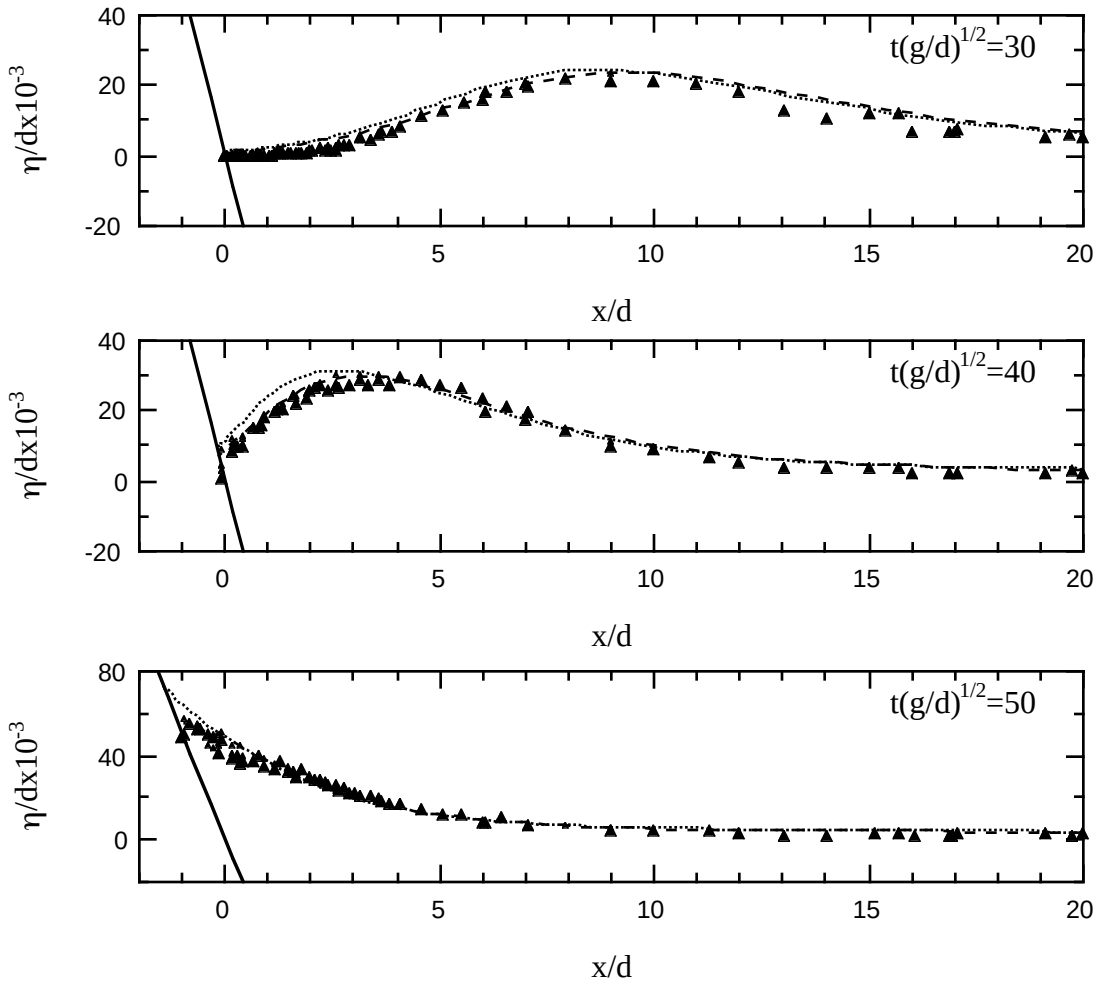

Figure 2.7 The runup of nonbreaking solitary wave with *H/d* = 0.019 on a 1:19.85 beach. The normalized surface elevation profiles are shown as a function of the normalized distance at five different times; the dotted line is the analytical solution, the dashed line is this numerical solution, and the points are the laboratory data of Synolakis (1987).

Equation (2.22) implies that crests of longer solitary waves were located further from the beach than those of shorter waves. This practice propagates solitary waves of different heights over identical relative distances until they climb the beach; since Synolakis (1987), it has been the standard convention for locating a solitary wave profile offshore for numerical models.

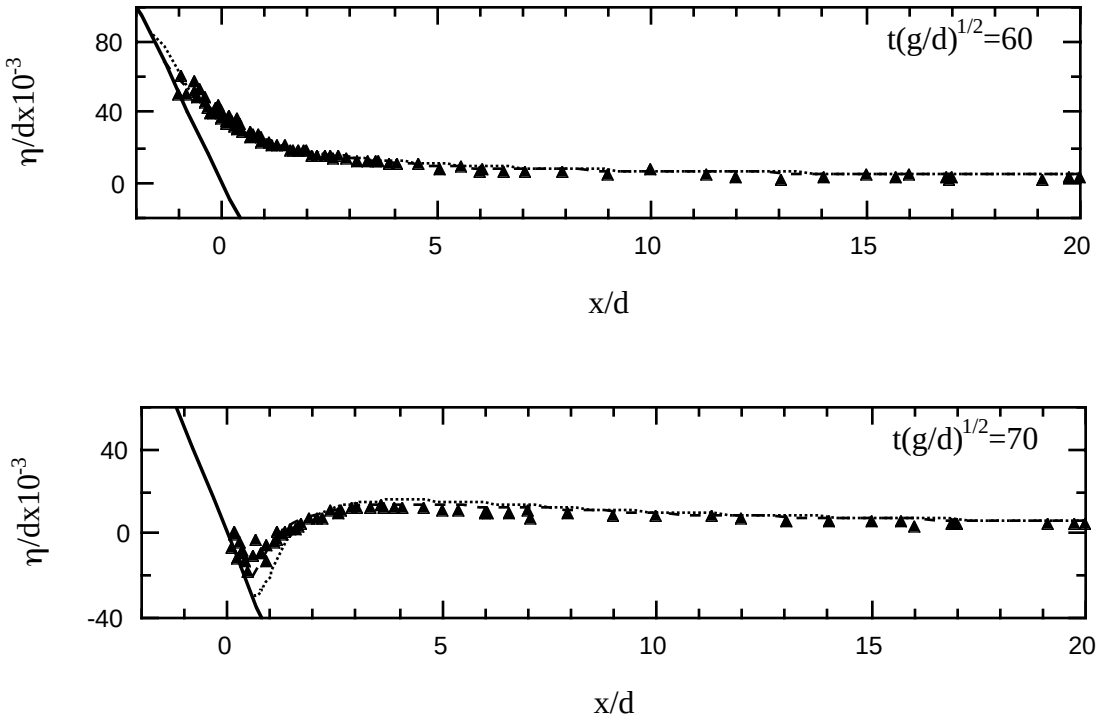

Figure 2.8 Same as in Figure 2.7

To evaluate the accuracy of the numerical method and specific features of the solution, different representations of the computed data were then compared with analytical and experimental results. Three types of representations are presented, time histories of surface elevations at specific locations, snapshots of the flow-field, i.e., wave profiles at fixed times as functions of the distance, and maximum runup data.

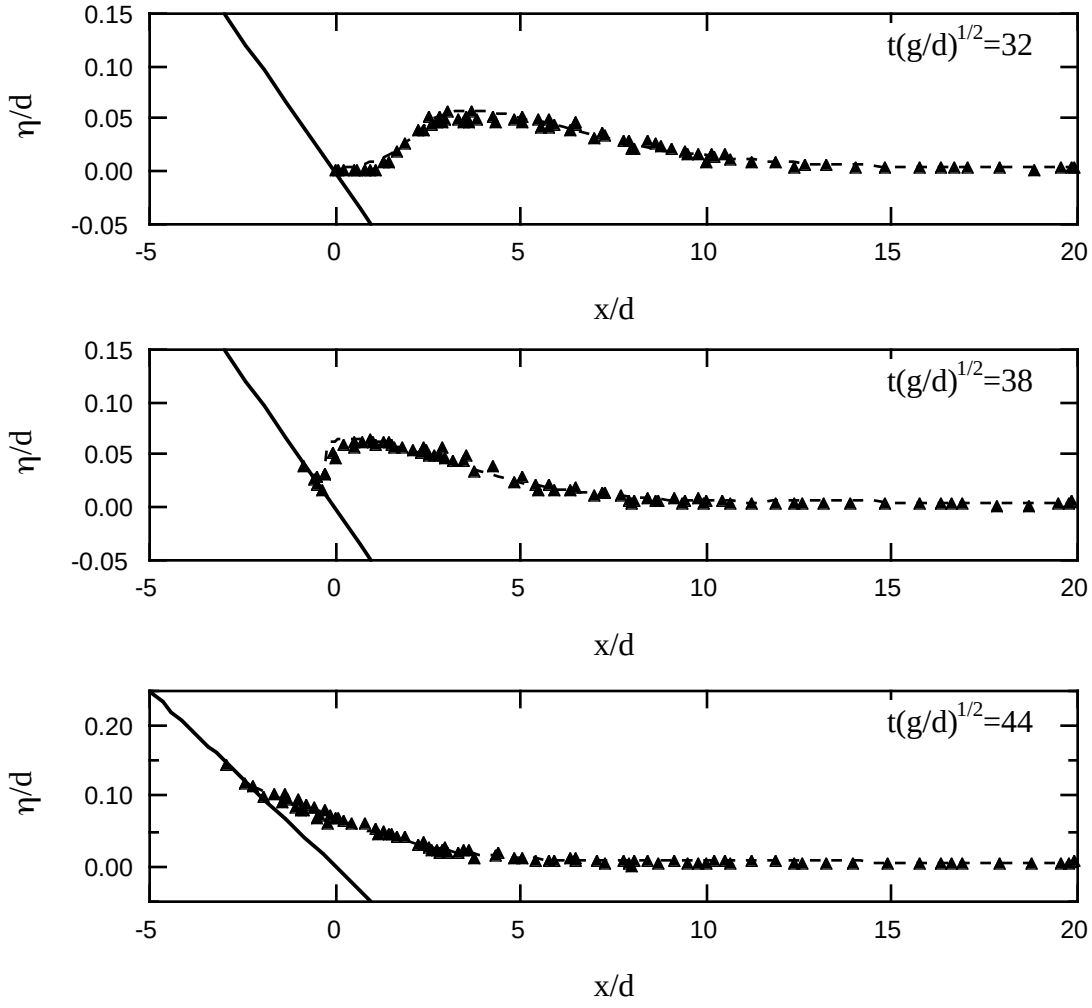

Figure 2.9 The evolution of a 0.019 nonbreaking solitary wave on a 1:19.85 beach. The dashed line is this numerical solution and the points are the laboratory data of Synolakis (1987).

Figure 2.6 – Figure 2.8 show the results for a solitary wave with initial amplitude $H/d = 0.019$ climbing over the beach with $\cot\beta = 19.85$. Figure 2.6 compares the computed waveforms with the analytical solution (Synolakis, 1987) at two different locations—near the initial shoreline, $x/d = 0.25$ and at $x/d = 9.95$, the midpoint between the shoreline and the toe of the beach. The agreement is quite good. Figure 2.7 and Figure 2.8 show a com-

parison among this numerical solution, the nonlinear analytical solution, and laboratory data. There is no significant differences between the three profiles. However, the figures show that the behavior of the numerical solution is closer to the experimental data than that of the analytical solution. This is a manifestation of numerical dissipation which is inadvertently introduced in any numerical computation, but yet it fortuitously improves the solution, at least in its ability to model the physical manifestation of the wave.

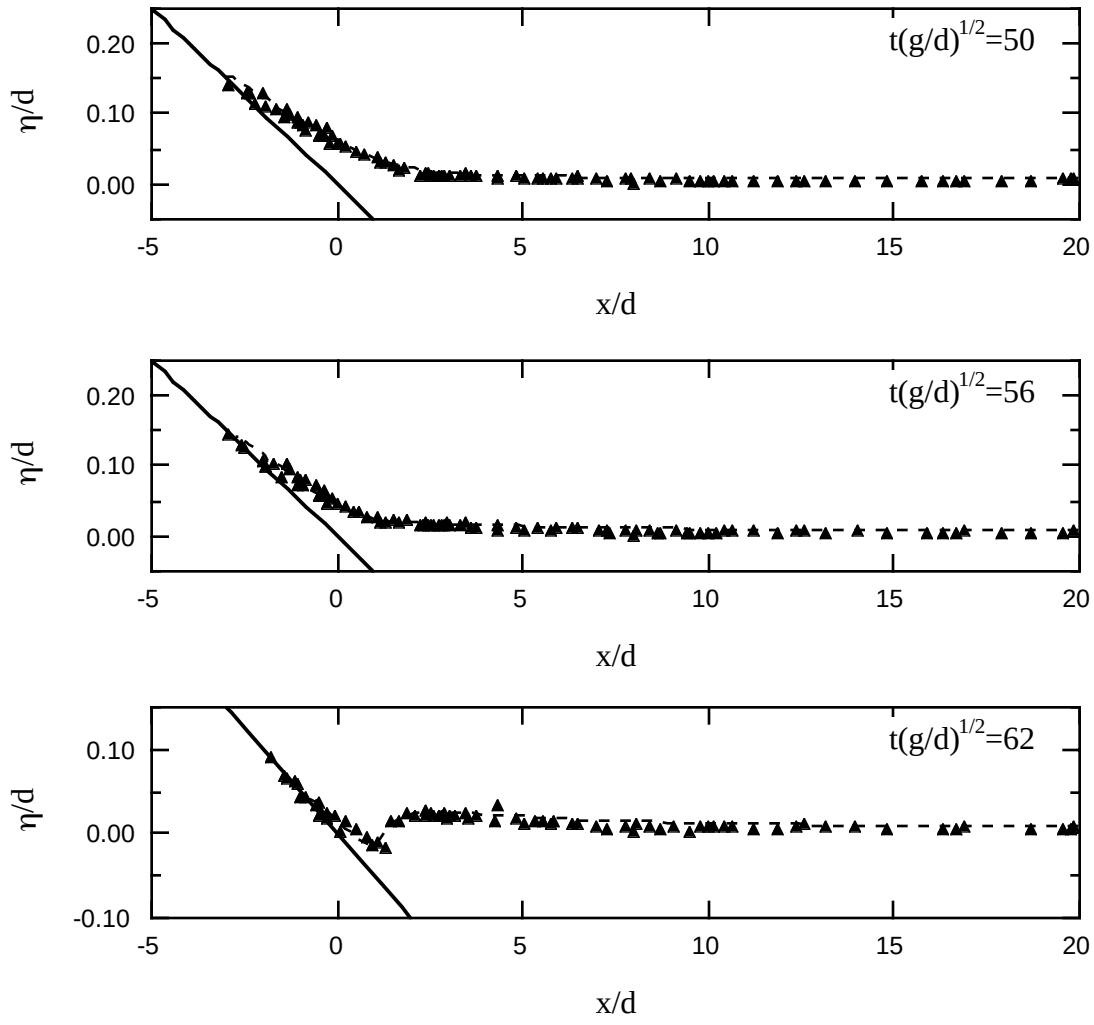

Figure 2.10 Same as in Figure 2.9

For the $\cot\beta$ = 19.85 beach, Synolakis' (1987) regularization of the Jacobian predicts that the shallow water theory becomes invalid during runup when H/d = 0.029. Figure 2.9 and Figure 2.10 show the evolution of a 0.04 wave, which is beyond that limiting value. This is a breaking wave in the nonlinear theory sense, i.e., the Jacobian is singular. Note, that this wave does not break in the laboratory (Synolakis, 1987); Meyer (1988 a, b) argued that the Jacobian regularization condition only fortuitously predicts wave breaking. Synolakis (1987) presented analytical results for this wave, and he commented how the robustness of the Carrier and Greenspan (1955) transformation allowed for the calculation of mildly breaking waves. The figures shows that the numerical solution is stable and in good agreement with the laboratory data, even though the profiles become almost vertical where the Jacobian becomes singular during runup and rundown, at $t\sqrt{g/d}$ = 38, and $t\sqrt{g/d}$ = 62 respectively.

The solitary wave with initial wave height H/d = 0.3 is clearly a nonlinear wave which plunges in the laboratory (Synolakis, 1986). The analytic solution becomes singular shortly after the wave starts climbing up the beach and consequently there are no analytical predictions. Figure 2.11, compares this numerical solution with the laboratory observations of Synolakis (1986) and with Zelt's (1991)'s finite-element numerical solution of Boussinesq equations. The profiles suggest that the computed wave breaks earlier than observed in the laboratory. The figure also suggests that the agreement between computed profiles and laboratory observations are not as good as the agreement with Zelt's (1991) calculations, which, however, include artificial viscosity and a friction factor. Zelt (1991) calcu-

lated his friction factor by varying it over a factor of five and choosing the value which produced the best agreement with the laboratory maximum runup data.

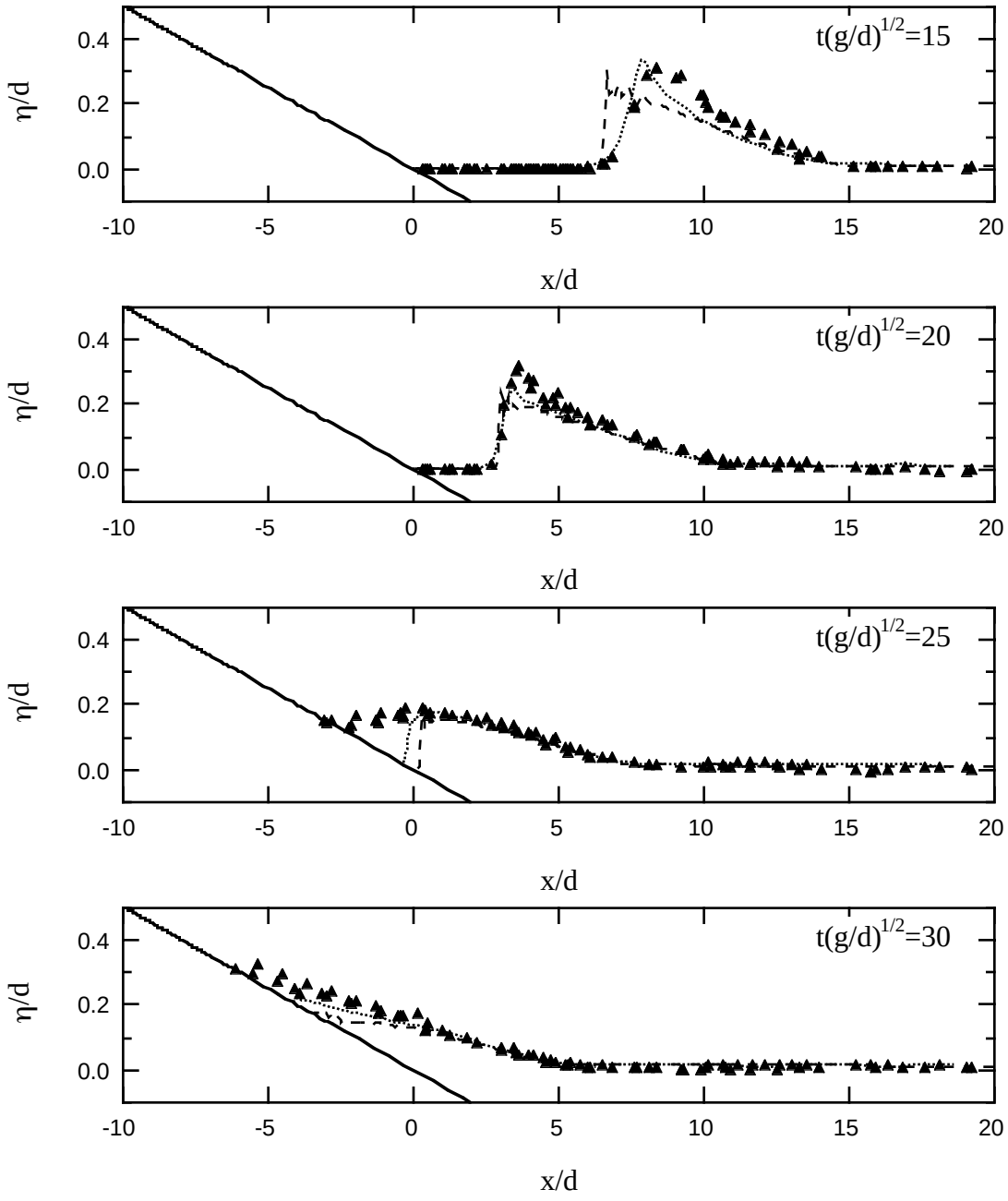

Figure 2.11 Evolution of a 0.3 breaking solitary wave on a 1:19.85 beach. Normalized surface elevation profiles are shown as a function of normalized distance at different times; dashed line is this finite-difference solution, dotted line is finite-element solution of Zelt (1991) and points are laboratory data of Synolakis (1987).

The breaking point in the numerical solution is determined as the point beyond which the wave amplitude begins to decrease. For the wave shown in Figure 2.11, this happens at $t\sqrt{g/d}$ = 14. The laboratory wave breaks between $t\sqrt{g/d}$ = 20 and $t\sqrt{g/d}$ = 25, just before runup on dry bed. Since the numerical scheme does not include artificial viscosity terms, the numerical solution experiences high-frequency oscillations behind the leading steep slope of the wave in Figure 2.11 at $t\sqrt{g/d}$ = 15 and 20. Nevertheless, the dissipative properties of the finite-difference scheme permit to continue computations. The numerical solution after breaking is stable and forms a realistic bore-type profile propagating toward the beach. Although, the breaking occurs earlier in the numerical computations, the processes of breaking and wave reforming are similar to the laboratory results. In fact, the profiles at time $t\sqrt{g/d}$ = 20 are quite similar. Both Zelt's and this numerical model do not reflect the details of breaking region during runup, as long wave models treat the plunging wave as a bore propagating up the slope (Figure 2.11 at $t\sqrt{g/d}$ = 25). However, since the momentum and mass are conserved, the numerical solutions are still able to reasonably model the runup process after breaking (Figure 2.11, $t\sqrt{g/d}$ = 30). Zelt's (1991) profiles are smoother than the finite-difference solution and they lag the laboratory profiles less. We believe that these differences in numerical solutions seem to be mostly due to the artificial viscosity used by Zelt in the vicinity of a bore, and not due to the difference in the field equations; it is unlikely whether the dispersive terms of the Boussinesq equations have sufficient time to affect the results in this fashion.

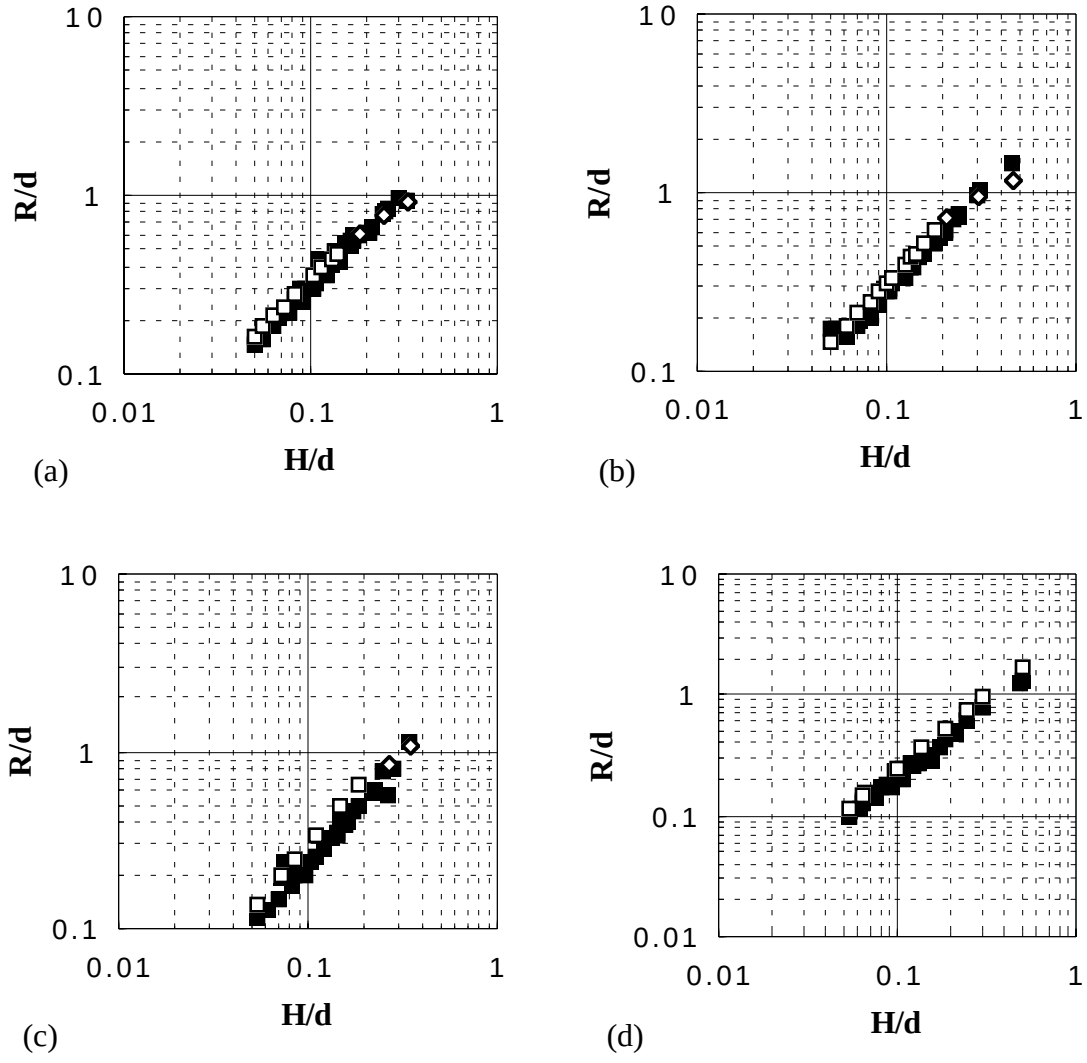

Figure 2.12 The normalized maximum runup of solitary waves up an (a) 1:5.67 beach, (b) 1:3.73, beach, (c) 1:2.14 beach, (d) 1:1 beach versus the normalized height of incident wave. Comparisons between VTSC-2 results (empty squares- nonbreaking data, empty diamonds- breaking detained the laboratory data of Hall & Watts (1953) (solid squares).

Another measure of the accuracy of the numerical solution is a comparison between computed values and laboratory maximum runup observations. Figure 2.12 and Figure 2.13

present the normalized maximum runup as a function of the normalized wave height for five different beaches, cotβ = 1, cotβ = 2.14, cotβ = 3.73, cotβ = 5.7 and cotβ = 20. The figures suggest that the maximum runup is predicted quite well both for breaking and non-breaking waves. In particular, Figure 2.13 clearly shows the change in slope between breaking and nonbreaking wave variations, first observed by Synolakis (1986, 1987).

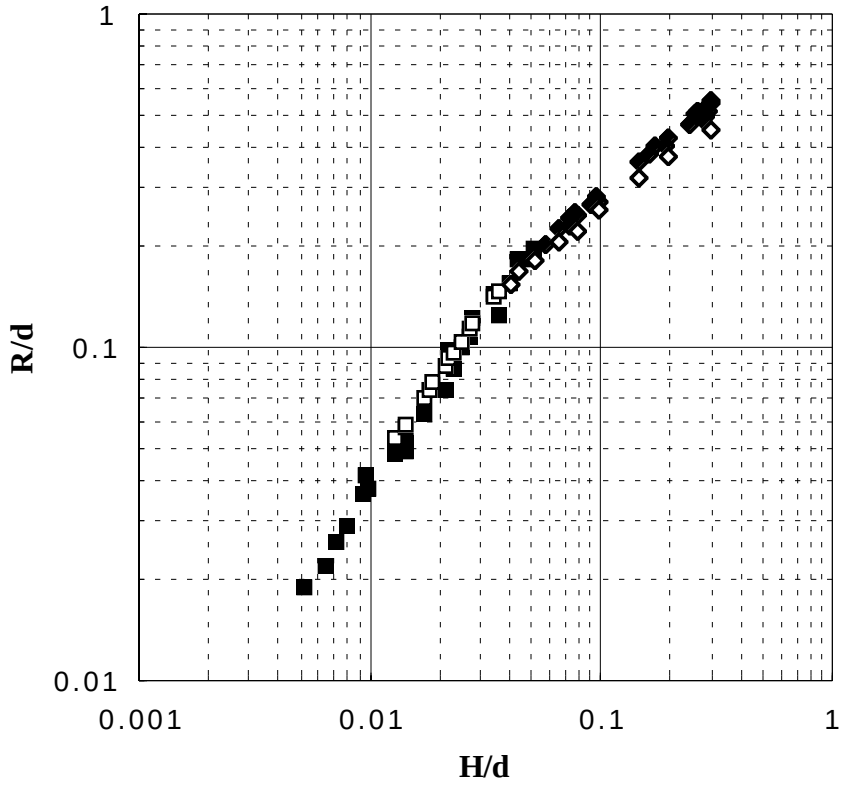

Figure 2.13 The normalized maximum runup of solitary waves up a 1:19.85 beach versus the normalized height. Comparisons among computer results (empty squares are for non-breaking data, empty diamonds are for breaking data) and the experiments of Synolakis (1987) (solid squares and diamonds).

This appears to be the first comprehensive numerical computation of maximum runup data; Kobayashi et al (1987,1989, 1992) calculated mostly the runup of breaking pe-

riodic waves on very rough slopes by introducing friction factors, making it difficult to assess his method for smooth slopes and for non-periodic waves. Zelt (1991) calculated only one runup value for the $H/d = 0.3$ wave on a 1:20 beach, the difficulty being that the friction factor was estimated from the maximum runup. Although it is unlikely that the friction factor would vary significantly among different solitary waves, Zelt does not comment if the friction factor has to be recomputed for different waves to attain the same level of accuracy as for the 0.30 wave.

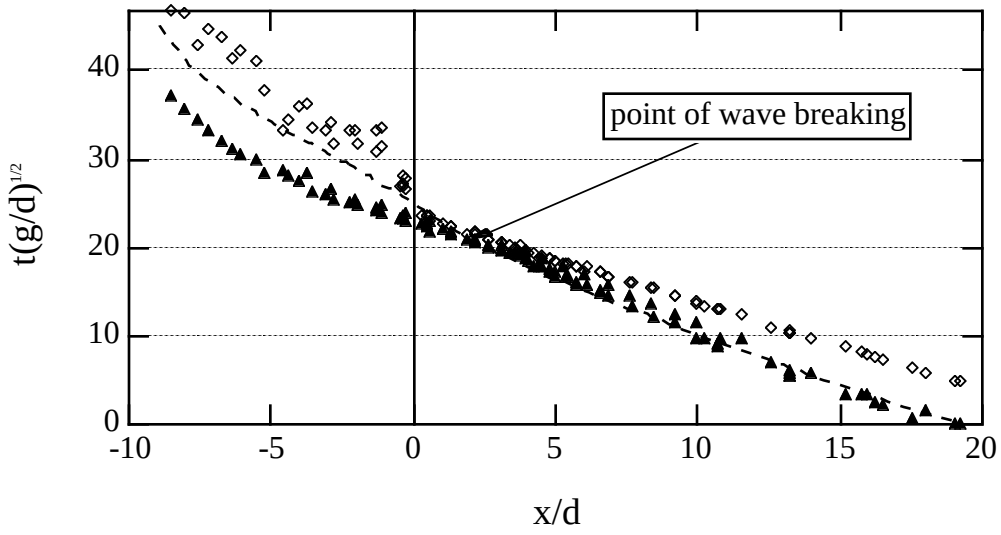

Figure 2.14 The evolution of the wave-front path (solid triangles) and of the wave-crest path (empty diamonds) in the laboratory, for a 0.30 solitary wave climbing a 1:19.85 beach The dashed line is VTSC-2's prediction of the evolution of the wave-front path.

To further investigate breaking wave evolution during shoaling and to understand the discrepancies between both computer models and the laboratory manifestation of the 0.3 breaking wave on Figure 2.11, we study the evolution of the wave front during runup.

The in Figure 2.14 shows a comparison between wave front path data and wave-crest path data from laboratory experiments (Synolakis, 1986, 1987a) and with the numerical computations for the 0.30 wave. The data indicate that once the wave breaks (approximately when the wave-crest and the wave-front paths meet, since the front face becomes almost vertical) the wave-front moves faster than before breaking. Note that, as Yeh et al (1989) found in their experiments of the runup of the laboratory manifestation of an infinite bore, once the wave breaks the wave moves faster on dry land. It can be seen, that beyond the initial shoreline, the two paths diverge again, also as indicated in figure 2 of Yeh et al (1989), where the distance between the shoreline (s) and front (f) points increases.

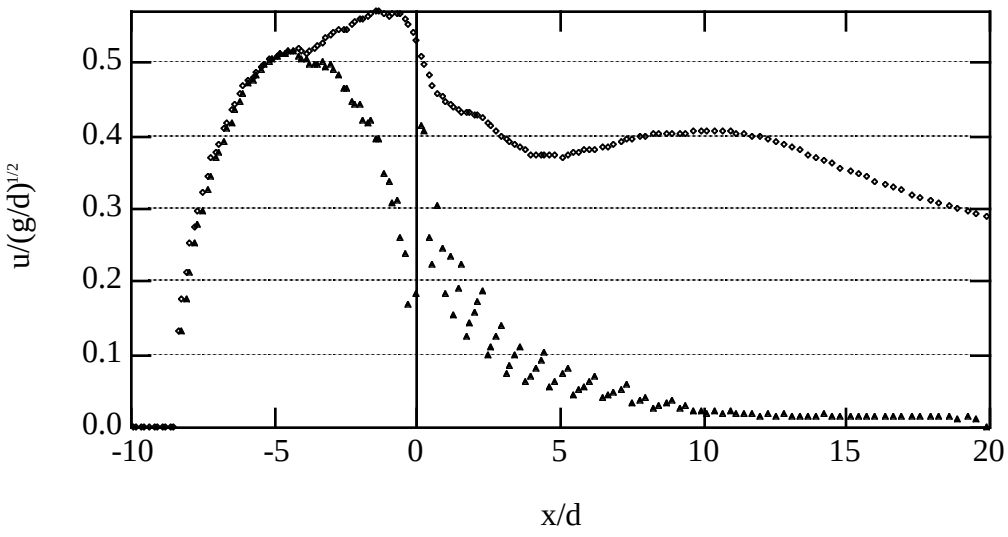

Figure 2.15 Computed dimensionless velocity of the wave-crest (diamonds) and wave-front (triangles) as a function of dimensionless distance for the 0.30 solitary wave of Figure 2.14.

Interestingly, the computed wave-front path follows predominantly the pattern of the wave-crest laboratory data on dry land ($x < 0$). This is also consistent with the experiments of Yeh et al (1989). They indicated that the actual front of a bore (which coincides

with the climbing wave-crest) follows behind a shoreline tip. Figure 2.15 shows computations of velocity of the wave front and wave crest. In the figure the offshore wave celerity is used for normalizing the velocity, in contrast to Yeh et al who use the classical bore velocity, which is only computable for the case of an infinite bore. Note however, that nonbreaking waves climb slower on dry land. (Synolakis, 1986, 1987b).

2.5 Summary and conclusions

A numerical solution of the shallow-water wave equations was presented, using an explicit second-order finite-difference scheme. An absorbing boundary condition was used to model the right boundary and a moving boundary condition was used to model the runup process. The variable computational grid for the finite-difference model substantially increases the efficiency of the numerical solution and its accuracy, since the number of nodes per wave length is almost constant everywhere in the area of computation. The comparisons with analytical and laboratory results show excellent agreement for nonbreaking waves (Figure 2.6–Figure 2.8). The computed results agree well with laboratory observations even for waves which in the nonlinear theory sense are breaking and which in nature break during the rundown (Figure 2.9–Figure 2.10). The computed results for plunging waves exhibit earlier breaking than the laboratory waves (Figure 2.11). The computed maximum runup for breaking waves is slightly smaller than observed (Figure 2.12 and Figure 2.13). The computed breaking wave profiles develop physically realistic bore-like profiles during runup.

The distinct advantage of this method is that it does not use any artificial viscosity or friction terms in the solution, therefore, there is no need for tuning the model for every wave type or bottom profile. The shoreline algorithm is simpler than the method Kobayashi et al (1987) and its derivatives. The entire solution algorithm is much simpler than Zelt's (1991) finite-element solution of the Lagrangian form of the Boussinesq equations. There is no difference with Zelt's results for nonbreaking waves; Zelt's breaking wave predictions lag the laboratory observations less than our results, but the computational expense of the finite element model and the self-calibration for obtaining the friction factor are severe limiting factors. VTCS-2 predicts equally good maximum runup values as the potential flow models, but again at a much smaller computational cost; all the results we presented here were computed on a Macintosh and every run took less then one minute including real time graphic animation. It is for this reason that we have been able to extend our method to two-dimensional topography. In the next chapter the method is extended to two plus one problem.